Applied Catalysis B: Environmental 202 (2017) 335–345

Contents lists available at ScienceDirect

Applied Catalysis B: Environmental

journal homepage: www.elsevier.com/locate/apcatb

Nano silica and molybdenum supported Re, Rh, Ru or Ir nanoparticles for selective solvent-free glycerol conversion to cyclic acetals with propanone and butanone under mild conditions

Maciej Kapkowski[a], Weronika Ambrożkiewicz[a], Tomasz Siudyga[b], Rafal Sitko[a], Jacek Szade[c], Joanna Klimontko[c], Katarzyna Balin[c], Józef Lelątko[d], Jaroslaw Polanski[a,*]

[a] Institute of Chemistry, University of Silesia, Szkolna 9, 40-006 Katowice, Poland
[b] Department of Chemistry, Silesian University of Technology, 44-100 Gliwice, Poland
[c] Institute of Physics, University of Silesia, 75 Pułku Piechoty 1A, 41-500 Chorzów, Poland
[d] Institute of Materials Science, University of Silesia, 75 Pułku Piechoty 1A, 41-500 Chorzów, Poland

ARTICLE INFO

Article history:
Received 24 June 2016
Received in revised form 27 August 2016
Accepted 16 September 2016
Available online 17 September 2016

Keywords:
Re, Ir, Rh, Ru nanoparticles
Glycerol acetalization
Heterogenous catalysis
Silica supported nanorhenium
Bimetallic Re/Mo, Ru/Mo, Rh/Mo, Ir/Mo

ABSTRACT

We described the preparation of a series of new catalysts, i.e., nano-silica supported Re, Ru, Ir, Rh NPs as well as various combinations of the above-mentioned metals as potential catalysts of glycerol acetalization with acetone or butanone for the first time. In fact, it was discovered that nano-SiO_2 supported Re in particular is a highly efficient selective catalyst of glycerol acetalization for five-membered cyclic acetals. While Re supported on nano-SiO_2 prefers five-membered cycles its replacement to Mo destroys this selectivity and both five- and six-membered products can be observed. Under optimal conditions, the TON that was observed significantly outperforms those that have been reported in the literature for other catalytic systems.

1. Introduction

Renewable naturally-sourced carbohydrates, amino acids and triglycerides are available in huge quantities in our environment. This biomass, which is a product of living organisms, could be used as valuable feedstock for chemical processing; however, we need *novel chemistry to selectively and efficiently transform large amounts in their natural state without extensive functionalization and protection* [1]. For this reason, biomass conversion has received increasing attention in contemporary chemistry. Glycerol, which is yielded as a byproduct in biodiesel production, is one of the most widely available biosourced chemicals, which makes it an attractive target of investigations. A variety of catalytic reactions have been developed, in particular, oxidation and dehydration [2,3]. Glycerol acetalization is an interesting alternative that can provide biodiesel additives, for example. The vast majority of reactions between polyols and ketones are performed by simply using strong inorganic or organic acids (H_2SO_4, HCl, HNO_3, dichloroacetic acid, *p*-toluenesulphonic acid) as catalysts [4,5], while other reactions are carried out in organic solvents, such as toluene [6], 1.4-dioxane [7], tetrahydrofuran [8], cyclohexane [9,10], dichloromethane [11]. These reactions can also be catalyzed by the complexes of d-block metals, e.g. Cu, Ir [6,12], metal oxides (ZrO_2) supported on silica or aluminosilicates [13,14], active carbon modified on the surface [7] or polymer fibers [9]. The majority of the procedures require a high temperature (70–110 °C) and a relatively long reaction time (3–6 h), whereas the degree of conversion ranges between 60 and 95% [6,7,13,14].

In particular, although the reaction of glycerol with acetone has been performed in the presence of various catalysts [15–18], it is usually done at temperatures higher than 60–70 °C. Recently, SBA-15-supported molybdenum phosphate [19], H-Beta zeolite [20] and heteropolyacid $H_3PW_{12}O_{40}$ [21] catalysts have been reported to actively promote the reaction of glycerol with acetone at room temperature.

From the chemical point of view, glycerol acetalization to cyclic acetals is an interesting example of a potential enhancement of catalytic-induced selectivity. For example, a reaction of glycerol with propanone (acetone) can result in two cyclic products of DDM – 2,2-dimethyl-1,3-dioxolane-4-methanol (solketal) and DDL

* Corresponding author.
E-mail address: polanski@us.edu.pl (J. Polanski).

http://dx.doi.org/10.1016/j.apcatb.2016.09.032
0926-3373/

– 2,2-dimethyl-1,3-dioxane-5-ol (Scheme 1). The catalysts that have been reported in the literature can prefer both products, e.g. DDM [22–27] or DDL [28]. Interestingly enough, the five-membered solketal cycle is preferred in the recently published studies [19,21].

In this study, we report silica-supported Re nanoparticles as a new, highly active and selective catalyst for glycerol acetalization at room temperature. In particular, this process allowed solketal with a ca. 100% glycerol conversion and ca. 100% selectivity to be obtained at room temperature. In order to further test catalytic activity, we additionally tested the reaction of glycerol with butanone. Both reactions, in particular, the one with butanone, have previously been investigated in the presence of heteropolyacid catalysts; however, the preparation of these were labor intensive, and the reaction with catalyst recovery appeared to need the addition of an extra toluene fraction [21]. Moreover, unlike a previous procedure [21] in which an excessive amount of ketone (glycerol to ketone amounted to 1:30) was needed to achieve high glycerol conversion (85% for acetone or 74% for butanone), our system appears to be active at a much lower amount of ketone, at the same time, yielding higher glycerol conversions and product selectivity.

2. Materials and methods

2.1. Preparation of Re and/or Ru and/or Rh and/or Ir NPs on sol-gel silica

The series of mono-, bi- and trimetallic Re, Ru, Rh, Ir silica supported nanocatalysts were prepared according to the optimized procedure. The carrier is obtained using the Stöber method [29] with tetraethyl orthosilicate (TEOS), which is added to a mixture of methanol and water with an aqueous ammonia solution [30]. A mixture was sonicated, then concentrated, dried, and reduced under hydrogen at 500 °C. In general procedure, a solution of anhydrous methanol (99.8% Sigma Aldrich) 1500 mL and 528 mL of 25 wt.% of ammonia solution (Chempur) were mixed with 305 mL of deionized water. After 10 min of stirring 100 mL of tetraethyl orthosilicate (99.0% Sigma Aldrich) was added to the reaction mixture which was next stirred for 5 h at room temperature. The colloidal silica suspension was centrifuged, placed in an ultrasound bath and stirred for 90 min. The resulting precipitate was washed with distilled water until a neutral pH were achieved (pH was determined using universal indicator paper). A solution containing Re and/or Ru and/or Rh and/or Ir precursor (Table S1, Supplementary material) in deionized water (10 mL) was added dropwise into the obtained carrier, i.e., colloidal silica, and stirred for 30 min. Next, it was dried at 60–90 °C for about 12 h in dark, ground and sieved. The reduction was conducted in an oven under hydrogen atmosphere at 500 °C for 4 h.

2.2. Preparation of bimetallic Re and/or Ru and/or Rh and/or Ir NPs on Mo carrier

Mono-, bi-, or trimetallic Re and/or Ru and/or Rh and/or Ir catalysts were prepared using a novel facile approach involving the transfer of nanoparticles from the intermediate carrier, i.e., SiO_2, to the target carrier. The general method includes several steps. The target carrier Mo, (10.00 g) and Re and/or Ru and/or Rh and/or Ir NPs of a low polydispersity deposited on the intermediate carrier, e.g., 1.0% Re/SiO_2, (10.10 g) were suspended in deionized water (80 mL) under mechanical stirring and sonication. After 10 min of vigorous stirring sodium hydroxide (23.3 mL 40% w/w) was added to the suspension and stirring was continued for 2 h at room temperature, whereupon the suspension was allowed to stand for about 18 h until the suspended solids sedimented. The suspension was centrifuged and the supernatant was decanted, the precipitate was washed eight times with deionized water and centrifuged again to achieve neutral pH of the supernatant. Precipitate was washed with deionized water, centrifuged and supernatant was removed. The obtained catalyst was dried in an electric dryer to a constant weight at 120 °C. The detailed data for all nanomaterials after transfer from the corresponding SiO_2 catalyst at Mo were collected in Table 2S, Supplementary material.

A content of metals in catalysts was given in wt%. In turn, the combinations of metal were prepared on the basis of molar ratio of individual metals, e.g., Re and Ru in the 1:1 Re/Ru.

2.3. Methods of catalysts characterization

The resulted preparations of silica and mono-, bi-, trimetallic silica or molybdate supported catalysts were examined by X-ray photoelectron spectroscopy (XPS) with the use of Prevac/VGScienta photoelectron spectrometer. Monochromatic AlKα x-ray radiation ($h\nu$ = 1486.7 eV) was used to obtain the photoelectron spectra of core levels of particular elements. The structure of the obtained XPS multiplets was analysed with the use of Multipak programme from Physical Electronics. Alternatively, the samples were suspended in ethanol, sonicated for 15 min and the resulted materials were deposited on carbon adhesive tape for the preparation of the samples for TEM analyses. The transmission electron microscopy (TEM) images of the resultant composites were obtained on a JEOL 2000 FX operating at 200 kV or high resolution (HRTEM) JEM 3010 microscopes (both with EDS systems for chemical composition microanalysis). The scanning electron microscopy (SEM) JSM 6480 or a PHILIPS XL 30 was used for morphology investigation of composite powders. The energy-dispersive X-ray fluorescence (EDXRF) analysis was performed on the Epsilon 3 spectrometer (Panalytical, Almelo, The Netherlands) with a Rh target X-ray tube with 50 μm Be window and max. power of 9 W. The spectrometer is equipped with

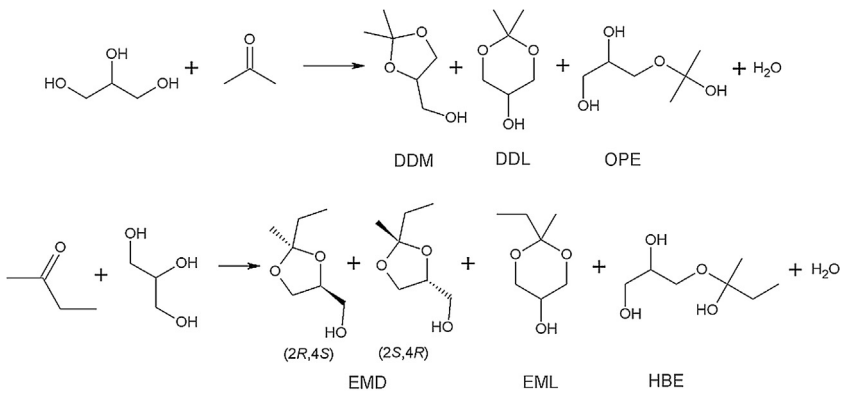

Scheme 1. Possible reaction products in direct glycerol acetalization with acetone or 2-butanone.

thermoelectrically cooled silicon drift detector (SDD) with 8 μm Be window and resolution of 135 eV at 5.9 keV. The quantitative analysis of mono-, bi-, or trimetallic Re and/or Ru and/or Rh and/or Ir catalysts at $-SiO_2$ or Mo was performed using Omnian software based on fundamental parameter method and following measurement conditions: 5 kV, 300 s counting time, helium atmosphere for Si determination; 12 kV, 300 s counting time, helium atmosphere, 50 μm Al primary beam filter (to remove peak of X-ray tube at low-energy region) for Rh; and 30 kV, 120 s counting time, air atmosphere, 100 μm Ag primary beam filter for Mo, Ru, Re and Ir. The current of the X-ray tube were fixed to not exceed dead-time loss of ca. 50%. The X-ray diffraction measurements were carried out using a Panalytical Empyrean diffractometer with Cu K_α radiation (40 kV, 30 mA) equipped with a PIXcel detector. Data were collected in the 10°–150° 2θ range with 0.0131° step. Qualitative phase analysis employed the "X'Pert High Score Plus" computer program and the data from ICDD PDF-4 database. Crystal lattice parameters were calculated using the Chekcell V4 program.

2.4. Acetalization

SiO_2 or Mo supported mono-, bi-, or trimetallic Re and/or Ru and/or Rh and/or Ir nanocatalysts 20–50 mg (1.0–4.9 μmol of Re and/or Ru and/or Rh and/or Ir) was suspended in a mixture 3.86/386.0/3860 mL (0.05/5/50 mol) of 99.0% acetone or 4.49 mL (0.05 mol) of 99.7% 2-butanone and 0.37/37.0/370.0 mL (0.005/0.5/5 mol) of 99.5% glycerol (Fisher BioReagents®—Glycerol For Molecular Biology) by sonication at room temperature for 10 min (RK 52 H, Bandelin Electronics, 35 kHz). Reagents were stirred at 200 or 300 rpm in a sealed tube (septa system) or round-bottomed flask with reflux placed in a thermostated oil bath at 25–55 °C for 0.5–3 h. The resulted reaction mixture was centrifuged and decantated. The supernatant was dissolved into deuterated water and analyzed using ^1H and ^{13}C NMR. Additionally, the 2D COSY and HMQC methods were used to identify and quantify products. The spectra were recorded on the Bruker Avance 400 or 500 spectrometers with TMS as internal standard (400 MHz, ^1H, 101 MHz ^{13}C or 500 MHz, ^1H, 126 MHz ^{13}C) at room temperature. The signal from water was suppressed using 90 water-selective pulses (zggpwg). The NMR analyses are much more clear if high purity glycerol was used as reagent, which in fact limits the possibility of this type of analytics here. Additionally, the GC-FID chromatography was used as the complementary technique. Product composition was determined by gas chromatography using HP gas chromatograph with a flame ionization detector FID (capillary column 60 m × 0.25 mm with DB-Wax as stationary phase, inlet temperature 250 °C; injection volume 0.5 μL; carrier gas He; oven temperature 150 °C; detector temperature 275 °C). Optionally this acetalization procedure was checked by another reaction 0.37 mL (5.0 mmol) of glycerol 99.5% with 4.49 mL (50.0 mmol) 2-butanone 99.7% in 55 °C for 1.5 h (300 rpm). Eqs. (1)–(6) were used to calculate conversion, product selectivity, yield, TON and TOF respectively. Selected NMR and GC-FID spectra with chemical shifts for the starting materials and products were presented in the Supplementary material, Fig. S1A-E, S2A-E.

$$Conversion(\%) = \frac{(initial\ moles\ of\ glycerol - final\ moles\ of\ glycerol)}{(initial\ moles\ of\ glicerol)} \times 100 \quad (1)$$

$$Selectivity(\%) = \frac{percentage\ amount\ of\ products\ formed}{the\ total\ percentage\ of\ all\ products\ formed} \times 100 \quad (2)$$

$$Yield(\%) = \frac{conversion \times selectivity}{100} \quad (3)$$

$$TON = \frac{n}{\alpha} \quad (4)$$

$$TOF = \frac{TON}{t}\left[h^{-1}\right] \quad (5)$$

$$TOF = \frac{\alpha}{n_{met} \cdot t}\left[h^{-1}\right] \quad (6)$$

Where *selectivity* - selectivity of desired product, n_{sub}—total number of moles of substrate, n_{met}—number of moles of nanometal(s), t—time in hours and α—system conversion degree.

3. Results and discussion

3.1. The catalysts preparation and structure

The EDXRF spectra of the catalysts studied show high intensity Si Kα or Mo Kα peaks at 1.74, 17.48 keV, respectively, as well as several peaks of the metal nanoparticles. The catalysts containing the Ru nanoparticles revealed peaks of the K series (Ru Kα and Ru Kβ at 19.28 and 21.66 keV, respectively), while the catalysts containing Rh nanoparticles showed both peaks of the K series (Rh Kα and Rh Kβ at 20.21 and 22.72 keV, respectively) as well as a low-energy Rh Lα1 peak of the L series at 2.70 keV. The EDXRF spectra of the Re-catalyst showed several peaks of the L series that corresponded to the L3 edge (Re Lα and Ll at 8.65, 7.60 keV), the L2 edge (Re Lβ1 and Lγ1 at 10.01, 11.69 keV) and the L1 edge (Lγ2,3 at 12.08 keV). Peaks for the L series were also observed for the Ir-catalysts: Lα at 9.18 keV (L3 edge), Lβ1 and Lγ1 at 10.71, 12.51 keV (L2 edge). The exemplary EDXRF spectra of Re-catalysts are shown in Fig. 1, while the quantitative analysis is presented in Table 1.

The X-ray diffraction patterns of 1.0 wt.% Re/SiO_2, 1.0 wt.% ReRu(1:1)/SiO_2, 1.0 wt.% ReRuIr(1:1:1)/SiO_2 and also SiO_2 samples are presented in Fig. 2. The patterns clearly showed peaks which could be attributed to metallic Ru, whereas only the most intensive peak for metallic Re was observed. Moreover, the overlapping of Re and Ru diffraction lines was noticed. Unfortunately, the Ir nanoparticles are below the sensitivity limit of XRD technique. The broad peak at low angle range is due to silica. The Scherrer equation was used to estimate the average size of crystalline particles. The particle size was estimated from the strongest diffraction lines ($2\theta_{101}$–44^0 for Ru NPs and $2\theta_{101}$–43^0 for Re NPs) and the values of about 5–6 nm were obtained for the all samples studied (Table 2).

In order to get insight into the chemical state of the active nanoparticles we analyzed the structure of the XPS core levels. One has to mention that due the limited inelastic mean free path of photoelectrons only the chemical state of the surface layers is reachable. The analysis depth is limited to about 2–4 nm. The structure of the XPS Re 4f level line is presented in Fig. 3a. Three spin-orbit doublets were fitted to the experimental spectrum. The lowest binding energy doublet can be assigned to metallic Re while the next one with the Re $4f_{7/2}$ line situated at about 44.3 eV is related to Re oxide. The literature data for Re oxides are rare and the values of binding energy are scattered. Thus the second doublet can be assigned to ReO_2 or to ReO_3. The energy position of the third doublet is higher than reported for the Re oxides. It may be connected to ReO_3 or to satellite lines which are common for transition elements compounds (Fig. 3a).

The analysis of the Ru lines in the Ru/Mo system is difficult due to the very weak intensity of Ru spectra and overlap of the most pronounced Ru lines with other elements present in the spectra – Mo and C. We analyzed the Ru $4p_{3/2}$ line which is shown in Fig. 3b. The low intensity line which can be attributed to metallic Ru is

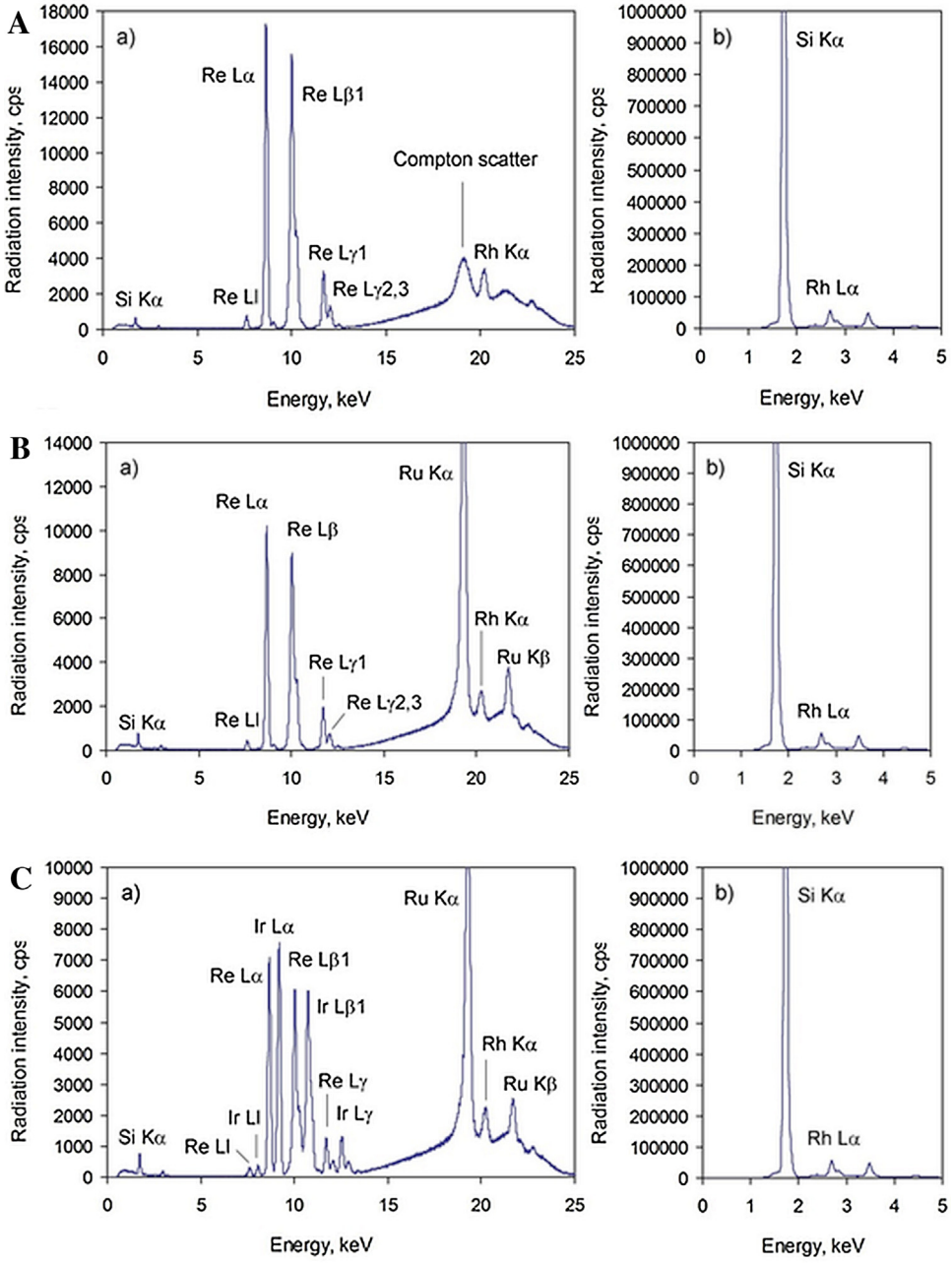

Fig. 1. EDXRF spectra of 1.0 wt.% Re/SiO_2 (A); 1.0 wt.% $RuRe/SiO_2$ (B); 1.0 wt.% $ReRuIr/SiO_2$ (C). a) Rh target X-ray tube operated at 30 kV and 300 μA, 100 μm Ag primary beam filter, air; b) Rh target X-ray tube operated at 5 kV and 1000 μA, helium.

visible at the lowest binding energy. The most intense line can be ascribed to RuO_2 while the lines visible at higher binding energies are possibly related to RuO_3. Similar structure can be obtained from the analysis of the Ru 3d doublet which is overlapping with the C 1 s line. One cannot exclude the presence of the Ru-Mo alloy which would have the binding energy similar to the metallic Ru. However, analysis of the Mo 3d doublet indicates only the oxidized state of this element, both MoO_2 and MoO_3 are present (Fig. 3c).

We used amorphous silica that had been synthesized using the sol-gel [30] technique as the basic carrier. SEM observations indicated that the silica obtained using this method exhibited a regular spherical shape, a controlled size distribution and a uniform porous surface (Fig. 4a–c). This regular shape was preserved in Re and/or Ru and/or Rh and/or Ir NPs supported on the SiO_2 carrier that was obtained using the Stöber method. In Re/SiO_2 catalyst the Re nanoparticles are distributed on the surface of SiO_2 surface. They are arranged individually and as conglomerates (Fig. 4a). The addition of Ru changed the structure of nanoparticles. The Re and Ru possesses the same structure (space group $P6_3/mmc$), similar atomic radius and their lattice parameter differ only slightly. Therefore they created particles of solid solutions [31] with the crystallite dimensions of about 10 ÷ 20 nm (Fig. 4c). The chemical composition of these particles changes in a wide range. The ReRu particles are inhomogeneous distributed on surface of SiO_2 (Fig. 4b). In larger clusters of particles some amount of amorphous Si were identified. The structure of molybdenum particles is visible in Fig. 4d. They have a regular shape and differ in size and include in the range of 1 ÷ 10 μm. On their surface the nanoparticles of Ru are located (Fig. 4e,f).

Table 1
EDXRF analysis of mono-, bi- and trimetallic Re, Ru, Rh, Ir catalysts deposited at SiO_2.

Catalyst	wt.%			
	Re	Ru	Rh	Ir
SiO_2	–	–	–	–
1.0% Re/SiO_2	0.95 ± 0.019	–	–	–
1.0% Ru/SiO_2	–	1.12 ± 0.023	–	–
1.0% Rh/SiO_2	–	–	1.14 ± 0.020	–
1.0% Ir/SiO_2	–	–	–	0.98 ± 0.023
1.0% ReRu(1:1)/SiO_2	0.55 ± 0.012	0.56 ± 0.010	–	–
1.0% RuRh(1:1)/SiO_2	–	0.50 ± 0.012	0.56 ± 0.021	–
1.0% ReRh(1:1)/SiO_2	0.51 ± 0.010	–	0.61 ± 0.011	–
1.0% ReIr(1:1)/SiO_2	0.53 ± 0.010	–	–	0.49 ± 0.016
1.0% RuIr(1:1)/SiO_2	–	0.55 ± 0.019	–	0.49 ± 0.010
1.0% RhIr(1:1)/SiO_2	–	–	0.60 ± 0.013	0.72 ± 0.010
1.0% ReIrRu(1:1:1)/SiO_2	0.34 ± 0.012	0.40 ± 0.015	–	0.28 ± 0.013
1.0% ReIrRh(1:1:1)/SiO_2	0.35 ± 0.010	–	0.39 ± 0.013	0.36 ± 0.010
1.0% RuIrRh(1:1:1)/SiO_2	–	0.40 ± 0.012	0.36 ± 0.013	0.31 ± 0.010
1.0% ReRuRh(1:1:1)/SiO_2	0.50 ± 0.022	0.31 ± 0.014	0.36 ± 0.015	–

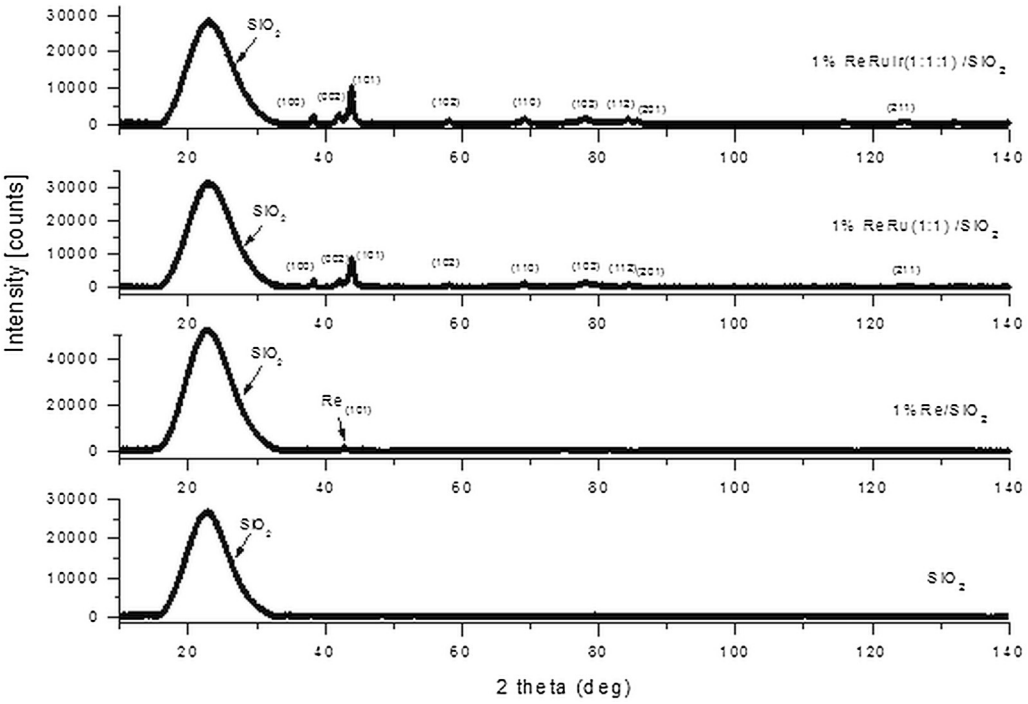

Fig. 2. The X-ray diffraction patterns of 1.0 wt.% Re/SiO_2, 1.0 wt.% ReRu(1:1)/SiO_2, 1.0 wt.% ReRuIr (1:1:1)/SiO_2 and SiO_2 samples. Miller indices for experimental peaks of Re and Ru NPs are marked.

3.2. Glycerol acetalization

Solvent-free conditions and mild reaction temperatures, which should be first of all inexpensive, have many potential advantages in the processing of waste glycerol. We previously showed that the glycerol concentration influences the viscosity of a system, which strongly controls the reagent contact with the catalyst surface during heterogeneous nanocatalysis on silica [32]. Therefore, we also decided to make this a priority when designing a solvent-free reaction system at the highest possible glycerol concentration.

Table 2
The average size of crystalline particles in investigated nanomaterials as determined by XRD method.

Catalyst	Lattice parameters [Å]	D[a] (nm) Re	D[a] (nm) Ru
SiO_2	–	–	–
1.0% Re/SiO_2	–	5.0	–
1.0% ReRu(1:1)/SiO_2	for Ru a = 2.715(±0.002) c = 4.297(±0.001)	6.0	6.5
1.0% ReRuIr(1:1:1)/SiO_2	for Ru a = 2.718 ± (0.002) c = 4.310 ± (0.003)	6.4	6.5

[a] Calculations for (101) diffraction line.

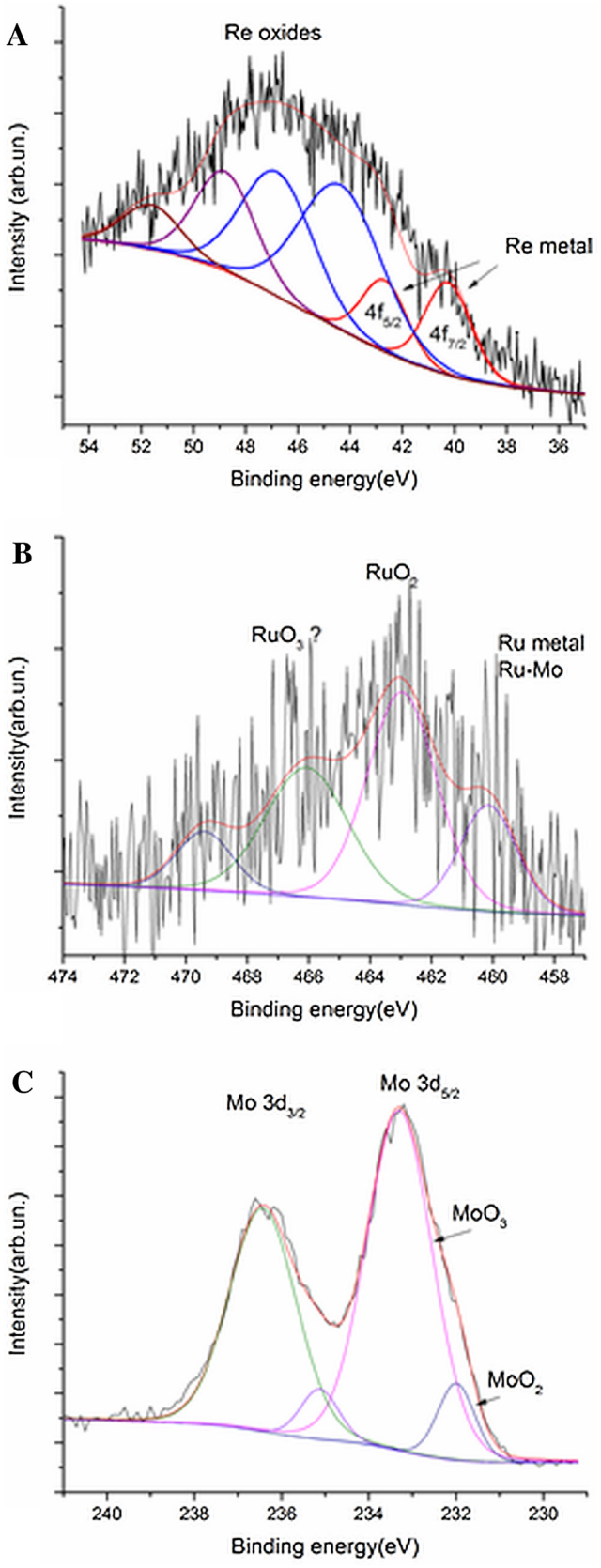

Fig. 3. XPS results for Re/SiO_2 (A) and Ru/Mo (B and C) systems. Panel A shows the Re 4f photoemission line together with the results of fitting. Analysis of the Ru 3p3/2 line and Mo 3d doublet is presented in panels B and C respectively.

For example, in comparison to the previous procedure, we managed to maintain a three times higher glycerol concentration. The molar ratio glycerol to ketone amounted to 1:10 in the current study vs. 1:30 in [21], whereas in practice, the reported procedure needed further dilution with toluene at a v/v ratio of ca. 1:1 to glycerol [21].

To create Table 3, we compared a series of systematic screening of nano-silica supported Re, Ru, Ir, Rh nanoparticles as well as various combinations of the above-mentioned metal NPs as potential catalysts of glycerol acetalization with acetone at 55 °C. These results indicate that at first the reaction did not proceed to cyclic acetals as is shown in Scheme 1 without the catalyst (Table 3, entry 1) or with nano-silica alone (Table 3, entry 2). In such conditions, the glycerol conversion was very low and did not exceed 8%. The highest catalyst performance was revealed for Re/SiO_2 (Table 3, entry 4) as single metal NPs, for which we observed a 100% glycerol conversion with a 94.1% selectivity to solketal. The high TON value of 1862.1 [mol mol^{-1}] compares advantageously to those calculated for reactions that have been reported in the literature, in particular, those calculated for Mo in 40% MoPO/SBA-15 TON = 47.5 [mol mol^{-1}] [19], for H-Beta-1 zeolite catalyst TON = 116 [mol mol^{-1}] [20] or for W in $H_3PW_{12}O_{40}$ TON = 7.5 [mol mol^{-1}] [21]. The reaction was further characterized by the TOF values recorded for the changing reaction time of 0.5, 3 and 20 h (Table S3, Supplementary material). For the nano-Re/SiO_2 system this takes a values of ca. 3724, 621 and 93 [h^{-1}], respectively. Moreover, the reaction practically failed when we tried to use the commercial 1.0% Re/SiO_2 (Riogen, conversion α = 3.9%).

The high performance of the Re/SiO_2 system can be further increased by combining Re with Ir, which provides a similar glycerol conversion of close to 100% but with a slightly higher selectivity of 96% and a TON value of 1891.6 [mol mol^{-1}] (Table 3, entry 10). Some other highly efficient combinations can be seen in Table 3; however, they were below the performances of the Re systems discussed above.

Molybdenum Mo is another catalytic system that has been tested as a potential catalyst for glycerol acetalization [27]. Therefore, to create Table 4, we screened other possible combinations of the Re, Ru, Ir, Rh, which were now supported on Mo grains. We used our previously reported method [32–34] for the synthesis of these catalytic systems. In this analysis, the Ru NPs and their combinations appeared to be the most active catalysts (Table 4, entries 3, 11, 13). Although the conversion could also reach 100%, the selectivity of the five- vs. six-membered cycle was much lower than the one observed for the silica-supported NPs, which means that in addition to DDM, we also observed a relatively high fraction of DDL.

To create Table 5, we specified the performance of the catalysts with the highest activity that had been identified from the screening that was performed for the glycerol-acetone system in the reaction of glycerol with butanone. The cyclic product of this reaction, which has two chiral carbons, can form two diastereomeric forms as was shown in Scheme 1. As was expected, these diastereomers were formed as an almost equimolar mixture. In this reaction, the new catalytic system Re/nano-SiO_2 appeared to be more or less one of the highest efficiency, providing more than a 92% glycerol conversion and a TON value of 1724 [mol mol^{-1}], which compares advantageously to the TON values calculated for W in $H_3PW_{12}O_{40}$ TON = 6.2 [mol mol^{-1}] in the literature [21].

Fig. 5 shows the influence of temperature on the conversion and selectivity of the solketal formation. This indicates that although glycerol reacts with propanone at room temperature (glycerol conversion reach ca. 100%), the cyclization to solketal is less selective than at a higher temperature of 55 °C. The main byproduct among other products (OPE) was an acyclic propanone adduct (selectivity up to 10.3%) or a six-membered cycle DDL (selectivity up to 12.5%). It is worth mentioning that at 35 °C, the content of the uncyclizied

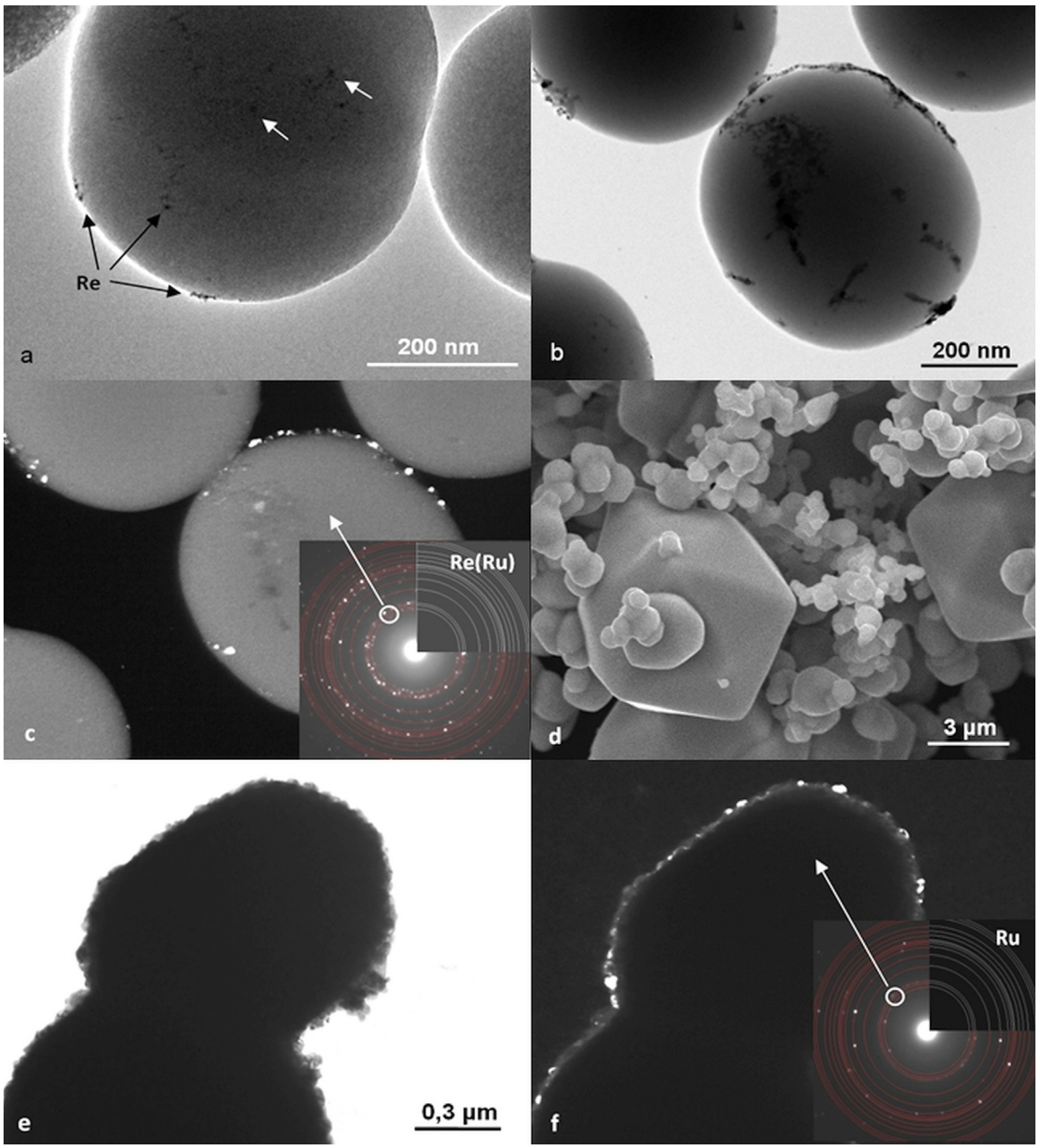

Fig. 4. Representative TEM (a–c,e,f) and SEM (d) images of the 1.0 wt.% Re/SiO_2, 1.0 wt.% ReRu(1:1)/SiO_2 and 1.0 wt.% Ru/Mo catalysts. a—nanoparticles of Re phase on surface of SiO_2 particles, b, c—nanoparticles of Re(Ru) phase on SiO_2 particles, d—structure of Mo microparticles and e, f—Ru nanoparticles on surface of Mo particles.

glycerol adduct was ca. 5.3% (Fig. 5). This can be further reacted by an increase in the duration of the reaction.

The recycle potential of the 1.0 wt.% Re/SiO_2 catalyst indicated that the efficiency of the system is almost fully retained for up to two cycles (Fig. 6). The main reason for the decrease in catalytic activity is the formation of glycerol polymers, which block the access to the catalyst. This effect depends on the individual catalysts and is especially noticeable at higher temperatures. Therefore, in the large-scale experiments at 35 °C, the catalyst appeared to retain its full catalytic activity without the need for any additional catalyst purification when tested for three cycles.

Since the investigated reactions are of interest to industries, we performed a larger scale experiment using the glycerol-acetone system (up to the 4 L scale). The content of the products that were yielded in the large-scale experiments was proven using gas chromatography (GC). The results are presented in Table 6. When the temperature was kept close to the ambient conditions (30 °C), both the conversion and selectivity remained high 100% (conversion) and 98% (solketal selectivity), despite a fact that the catalyst content was reduced up to 60% in comparison to the small-scale experiments.

3.3. *Synergy effects between Re, Ru, Rh, Ir NPs supported at SiO_2 or Mo*

Multicomponent composite heterogeneous catalysis was tested extensively to achieve more satisfactory catalytic performance for enhanced activity and/or selectivity. In such systems cooperation between different components or active sites in one catalyst can significantly enhance or reduce catalytic performance of individual components in synergistic enhancement [35] or synergistic inhibition [36], respectively. We tested here the potential synergy in

Table 3
Catalytic performance of SiO_2 supported Re, Ru, Ir, Rh NPs in glycerol acetalization with acetone at 55 °C.[a]

	Catalyst	α[b] [%]	TON[c]	TOF[c] (h^{-1})	TOF[d] (h^{-1})	Selectivity [%][b]			Yield [%][b]		
						DDM	DDL	OPE	DDM	DDL	OPE
1	None	3.6	0	0	0	0	0	100	0	0	3.6
2	SiO_2	3.6	0	0	0	0	0	100	0	0	3.6
3	1.0% Ru/SiO_2	16.0	161.7	53.9	10.8	52.6	26.3	21.1	8.4	4.2	3.4
4	1.0% Re/SiO_2	100	1862.1	620.7	124.1	94.1	2.7	3.2	94.1	2.7	3.2
5	1.0% Rh/SiO_2	3.4	35.0	11.7	2.3	0	0	100	0	0	3.4
6	1.0% Ir/SiO_2	2.9	55.7	18.6	3.7	0	0	100	0	0	2.9
7	1.0% ReRu(1:1)/SiO_2	100	1310.2	436.7	87.3	93.4	1.9	4.7	93.4	1.9	4.7
8	1.0% RhRe(1:1)/SiO_2	4.8	63.6	21.2	4.2	0	0	100	0	0	4.8
9	1.0% IrRh(1:1)/SiO_2	3.8	50.9	17.0	3.4	0	0	100	0	0	3.8
10	1.0% ReIr(1:1)/SiO_2	100	1891.6	630.5	126.1	96.0	2.0	2.0	96.0	2.0	2.0
11	1.0% RhRu(1:1)/SiO_2	5.5	56.1	18.7	3.7	22.4	22.4	55.2	1.2	1.2	3.0
12	1.0% RuIr(1:1)/SiO_2	4.3	57.0	19.0	3.8	0	0	100	0	0	4.3
13	1.0% RuRhIr(1:1:1)/SiO_2	100	1221.2	407.1	81.4	93.5	2.8	3.7	93.5	2.8	3.7
14	1.0% ReRuIr(1:1:1)/SiO_2	100	1480.6	493.5	98.7	91.7	2.8	5.5	91.7	2.8	5.5
15	1.0% ReRhIr(1:1:1)/SiO_2	100	1493.5	497.8	99.6	92.4	2.0	5.6	92.4	2.0	5.6
16	1.0% ReRhRu(1:1:1)/SiO_2	100	1213.0	404.3	80.9	94.3	2.9	2.8	94.3	2.9	2.8

[a] 1.23 mol/L of glycerol in the reaction mixture (glycerol/acetone molar ratio 1:10), 50 mg of catalyst (1.8–4.9 μmol Re and/or Ru and/or Rh and/or Ir), inert reaction atmosphere (N_2), ultrasounds 10 min, 55 °C, 3 h, 200 rmp.
[b] DDM—2,2-dimethyl-1,3-dioxolane-4-methanol; DDL—2,2-dimethyl-1,3-dioxane-5-ol; OPE—3-(2-oxidanylpropan-2-yloxy)propane-1,2-diol (Scheme 1); α—system conversion degree.
[c] Turnover number (TON) or turnover frequency (TOF) calculated based on Eqs. (4)–(5).
[d] Turnover frequency (TOF) calculated based on Eq. (6).

Table 4
Catalytic performance of Mo supported Re, Ru, Ir, Rh NPs in direct glycerol acetalization with acetone at 55 °C.[a]

	Catalyst	α[b] [%]	TON[c]	TOF[c] (h^{-1})	TOF[d] (h^{-1})	Selectivity [%][b]			Yield [%][b]		
						DDM	DDL	OPE	DDM	DDL	OPE
1	None	3.6	0	0	0	0	0	100	0	0	3.6
2	Mo	7.2	0	0	0	0	0	100	0	0	7.2
3	1.0% Ru/Mo	100	1010.7	336.9	67.4	78.9	2.4	18.7	78.9	2.4	18.7
4	1.0% Re/Mo	20.1	374.3	124.8	25.0	47.8	25.1	27.1	9.6	5.0	5.4
5	1.0% Rh/Mo	39.0	401.3	133.8	26.8	75.0	18.8	6.2	29.3	7.3	2.4
6	1.0% Ir/Mo	47.5	913.0	304.3	60.9	72.8	5.1	22.1	34.6	2.4	10.5
7	1.0% ReRu(1:1)/Mo	26.8	351.1	117.0	23.4	60.1	29.0	10.9	16.1	7.8	2.9
8	1.0% ReIr(1:1)/Mo	57.6	1089.6	363.2	72.6	73.5	17.6	8.9	42.3	10.1	5.1
9	1.0% RhRe(1:1)/Mo	4.3	57.0	19.0	3.8	0	0	100	0	0	4.3
10	1.0% RuIr(1:1)/Mo	27.8	368.3	122.8	24.6	50	24.1	25.9	13.9	6.7	7.2
11	1.0% RuRh(1:1)/Mo	100	1019.8	339.9	68.0	93.4	0	6.6	93.4	0	6.6
12	1.0% IrRh(1:1)/Mo	8.3	111.3	37.1	7.4	36.7	22.2	41.1	3.0	1.8	3.4
13	1.0% RuRhIr(1:1:1)/Mo	100	1221.2	407.1	81.4	89.8	1.6	8.6	89.8	1.6	8.6
14	1.0% ReRuIr(1:1:1)/Mo	16.7	247.3	82.4	16.5	50.0	28.5	21.5	8.4	4.8	3.6
15	1.0% ReRhIr(1:1:1)/Mo	100	1493.5	497.8	99.6	90.4	1.9	7.7	90.4	1.9	7.7
16	1.0% ReRhRu(1:1:1)/Mo	27.2	329.9	110.0	22.0	62.6	28.3	9.1	17.0	7.7	2.5

[a] 1.23 mol/L of glycerol in the reaction mixture (glycerol/acetone molar ratio 1:10), 50 mg of catalyst (1.8–4.9 μmol Re and/or Ru and/or Rh and/or Ir), inert reaction atmosphere (N_2), ultrasounds 10 min, 55 °C, 3 h, 200 rmp.
[b] DDM—2,2-dimethyl-1,3-dioxolane-4-methanol; DDL—2,2-dimethyl-1,3-dioxane-5-ol; OPE—3-(2-oxidanylpropan-2-yloxy)propane-1,2-diol (Scheme 1); α—system conversion degree.
[c] Turnover number (TON) or turnover frequency (TOF) calculated based on Eqs. (4)–(5).
[d] Turnover frequency (TOF) calculated based on Eq. (6).

Table 5
Catalytic performance of SiO_2 and Mo supported Re and Ru NPs in direct glycerol reaction with 2-butanone at 55 °C.[a]

	Catalyst	α[b] [%]	TON[c]	TOF[c] (h^{-1})	TOF[d] (h^{-1})	Selectivity [%][b]		Yield [%][b]	
						EMD	OS	EMD	OS
1	None	0.3	0	0	0	100	0	0.3	0
2	SiO_2	0.6	0	0	0	100	0	0.6	0
3	Mo	0.3	0	0	0	100	0	0.3	0
4	1.0% Re/SiO_2	92.6	1724.3	1149.5	115.0	94.6	5.4	87.6	5.0
5	1.0% Ru/Mo	67.1	678.2	452.1	45.2	93.4	6.6	62.7	4.4

[a] 1.04 mol/L of glycerol in the reaction mixture (glycerol/2-butanone molar ratio 1:10), 50 mg of catalyst (2.7 μmol Re or 4.9 μmol Ru), inert reaction atmosphere (N_2), ultrasounds 10 min, 55 °C, 1.5 h, 300 rmp.
[b] EMD—(2-ethyl-2-methyl-1,3-dioxolan-4-yl)methanol; OS—other products (EML—2-ethyl-2-methyl-1,3-dioxan-5-ol or HBE—3-[(2-hydroxybutan-2-yl)oxy]propane-1,2-diol)—structures shown in Scheme 1; α—system conversion degree.
[c] Turnover number (TON) or turnover frequency (TOF) calculated based on Eqs. (4)–(5).
[d] Turnover frequency (TOF) calculated based on Eq. (6).

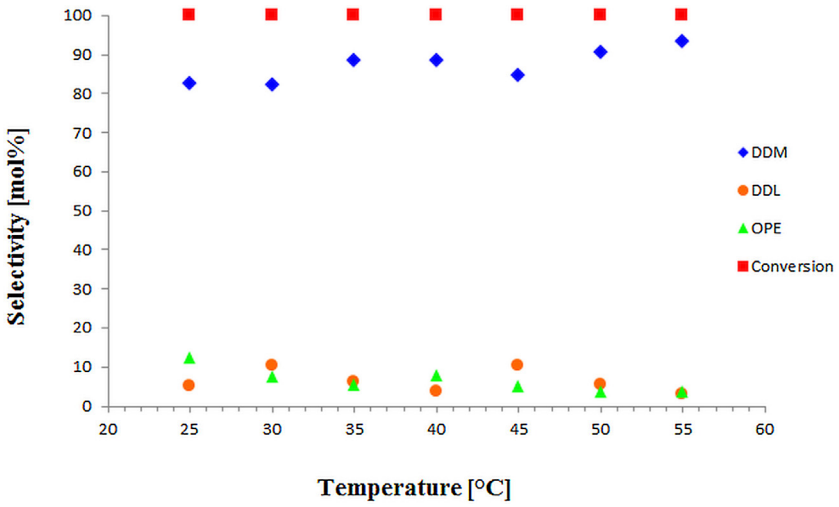

Fig. 5. Yield and conversion degree of solketal and byproducts received at various temperatures for 1.0 wt.% Re/SiO_2 catalyst. Reaction conditions: 1.23 mol/L of glycerol in the reaction mixture (glycerol/acetone molar ratio 1:10), 20 mg of catalyst (1.1 μmol Re), inert reaction atmosphere (N_2), ultrasounds 10 min, 55 °C, 1.5 h, 200 rpm. DDM (blue)—2,2-dimethyl-1,3-dioxolane-4-methanol (solketal); DDL (orange)—2,2-dimethyl-1,3-dioxane-5-ol; OPE (green)—3-(2-oxidanylpropan-2-yloxy)propane-1,2-diol, (red)—system conversion degree—α.

multicomponent Re, Ru, Rh, Ir NPs compositions supported on SiO_2 or Mo which were prepared by combining individual NPs at low temperature, therefore, not alloyed conjugates should be expected as the products. In fact, XPS analyses showed, that the bi- and tri-element combinations did not alloy even if components crystallize in the same crystallographic configuration. For example, the XRD indicated that in the 1.0% ReRu(1:1)/SiO_2 catalyst both Re and Ru NPs crystallized in hexagonal configuration ($P6_3/mmc$).

In Fig. 7 we illustrated the influence of various combinations of Re, Ru, Rh, Ir NPs on glicerol acetalization. All catalytic systems contained 1.0 wt.% of Re and/or Ru and/or Rh and/or Ir NPs as 1 or 1:1 or 1:1:1 (molar ratio) in mono-, bi-, or trimetallic combinations, respectively. In particular, Fig. 7a (SiO_2 supported) and Fig. 7b (Mo supported) allows us to better understand interaction effects between the metals investigated. The pie charts represent here the selectivity of the obtained products, namely, DDM (red), DDL (green) and intermediates OPE (yellow). Additionally, the conversion degree values (α) were given within the plots.

Silica supported catalysts appeared to be the most effective for all tested systems Fig. 7a. Especially, for Re NPs and their combinations ReRu, ReIr, ReRuIr, ReRhIr, ReRhRu we observed ca. 100% conversion degree with high selectivity of solketal formation (ca. 91–96%). Much worse efficiency was observed for Ru NPs where α amounted to 16% and the selectivity of solketal formation was ca. 52%. Even smaller activity was provided by Rh or Ir NPs where α was 2.9% and 3.4%, respectively and only the intermediate product OPE was formed. Moreover, the interaction between RhRe (α = 4.8%) and RhRu (α = 5.5%) resulted in the suppression of the Re or Ru activity, namely, the solketal selectivity decreased here from 94% to 0% and from 52.2% to 22.4%, respectively in comparison to Re (α = 100%) or Ru (α = 16%) monometallic catalysts. In addition, the enhancement or inhibition were observed if Ir was added to Re and Ru monometallic catalysts. Namely, the conversion degree for the

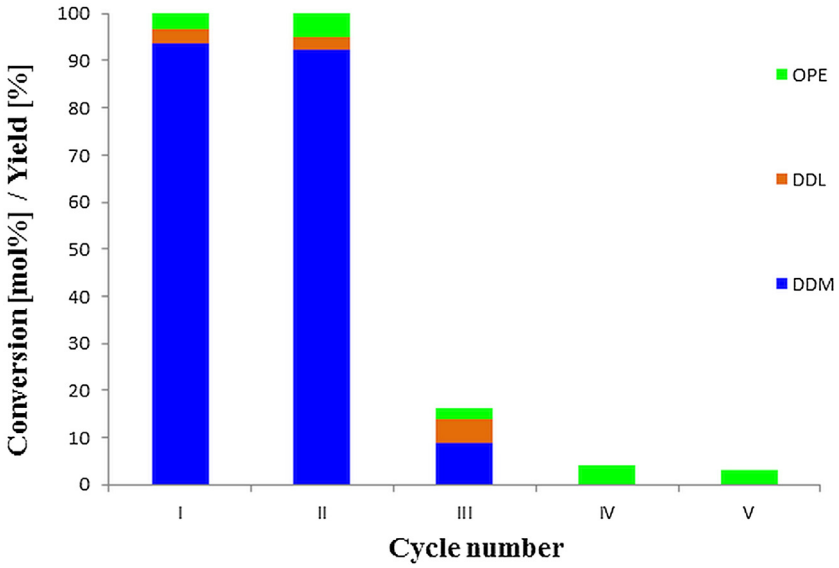

Fig. 6. Catalyst reuse experiment for 1.0 wt.% Re/SiO_2. Reaction conditions: 1.23 mol/L of glycerol in the reaction mixture (glycerol/acetone molar ratio 1:10), 50 mg of catalyst (2.7 μmol Re), inert reaction atmosphere (N_2), ultrasounds 10 min, 55 °C, 1.5 h, 200 rpm. DDM (blue)—2,2-dimethyl-1,3-dioxolane-4-methanol (solketal); DDL (brown)—2,2-dimethyl-1,3-dioxane-5-ol; OPE (green)—3-(2-oxidanylpropan-2-yloxy)propane-1,2-diol.

Table 6
Catalytic performance for the reuse experiment of 1.0% Re/SiO_2 catalyst in direct glycerol acetalization with acetone at 30 °C in scale 4.10–4100 mL.[a]

Test	Catalyst [mg]	α[b] [%]	Selectivity [%][b]			Yield [%][b]		
			DDM	DDL	OPE	DDM	DDL	OPE
I	20[c]	100	97.3	1.8	0.9	97.3	1.8	0.9
II		100	98.0	1.3	0.7	98.0	1.3	0.7
III		100	97.8	1.5	0.8	97.8	1.5	0.8
I	200[d]	100	96.5	2.3	1.3	96.5	2.3	1.3
II		100	97.0	2.1	0.8	97.0	2.1	0.8
III		100	96.9	2.0	1.0	96.9	2.0	1.0
I	2000[e]	100	98.3	0.2	1.4	98.3	0.2	1.4
II		100	97.2	1.1	1.7	97.2	1.1	1.7
III		87.3	98.1	0.6	1.3	85.7	0.5	1.2

[a] 1.23 mol/L of glycerol in the reaction mixture (glycerol/acetone molar ratio 1:10), inert reaction atmosphere (N_2), ultrasounds 10 min, 30 °C, 1 h, 200 rpm.
[b] DDM—2,2-dimethyl-1,3-dioxolane-4-methanol; DDL—2,2-dimethyl-1,3-dioxane-5-ol; OPE—3-(2-oxidanylpropan-2-yloxy)propane-1,2-diol (Scheme 1); α—system conversion degree.
[c] Test in scale 4.10 mL.
[d] Test in scale 410 mL.
[e] Test in scale 4100 mL.

ReIr catalyst amounted to α = 100% in comparison with monometallic Ir (α = 2.9%), Re (α = 100%) catalysts. The conversion degree α of 4.3% for the RuIr system took a value of to 4.3%, i.e., between these observed for the individual components Ru (α = 16%) or Ir (α = 2.9%). At the same time the addition of Ir slightly increased the solketal selectivity to 96% from ca. 94% (Re). In turn, the combination of Ir with Ru decreased the solketal selectivity from 52.2% (Ru) to 0% for RuIr system. In all trimetallic systems ReRuIr, ReRhRu, ReRhIr and RuRhIr a high conversion (α = 100%) was accompanied also by a high solketal selectivity (up to 90%). In these cases inactive bimetallic systems were activated by the presence of the additional components, e.g., the inactive RhRe was activated by the addition of Ru and Ir.

Molybdenum supported systems were the second group of materials prepared. The results of glycerol acetalization for these materials were presented in Fig. 7b. On average, the conversions and solketal selectivity here were lower vs. the SiO_2 supported systems. Moreover, a formation of a six-membered product (DDL) often accompanied here the conversion to solketal, a five-membered product. In particular, the highest conversion degree α of ca. 100%, was observed for Ru NPs/Mo system which promoted mainly a formation of solketal with selectivity of ca. 78%. The system of Ir NPs on Mo gave similar results of solketal selectivity ca. 73% however at the conversion degree α = 47.5%. In turn, Rh (α = 39.0%) and Re (α = 20.1%) provided similar solketal selectivity 75.0% and 47.8%, respectively. At the same time, the DDL fractions yielded here amounted to 18.8% for Rh or 25.1% for Re. For Mo supported catalysts with bimetallic NP systems both synergy (ReIr, RuRh) and inhibition (ReRu, IrRh, RuIr, RhRe) was observed. In particular, positive synergy was observed for ReIr catalyst where conversion degree increased to α = 57.6%. The DDM/DDL selectivity ratio increased here in comparison to the pure Re or Ir molybdenum supported catalysts. In the Mo supported three-component series the most effective catalyst of the highest solketal selectivity (ca. 90%) was ReRhIr and RuRhIr (α = 100%). In these cases Re or Ru NPs were activated by Rh or Ir NPs, respectively. In turn, the deactivation effect was observed for ReRuIr (α = 16.7%) catalyst in comparison with ReIr (α = 57.6%), ReRu (α = 26.8%) and Re (α = 20.1%). The comparison of the ReRhRu (α = 27.2%) and ReRu (α = 26.8%) systems indicated similar activity, but for RuRh (α = 100%) we observed much higher fractions of the main product—DDM.

A question appears if the observed catalytic activity can be correlated to the electronic state of the catalyst. For metals in group VIII–XI the catalytic activity is partially due to the degree of the

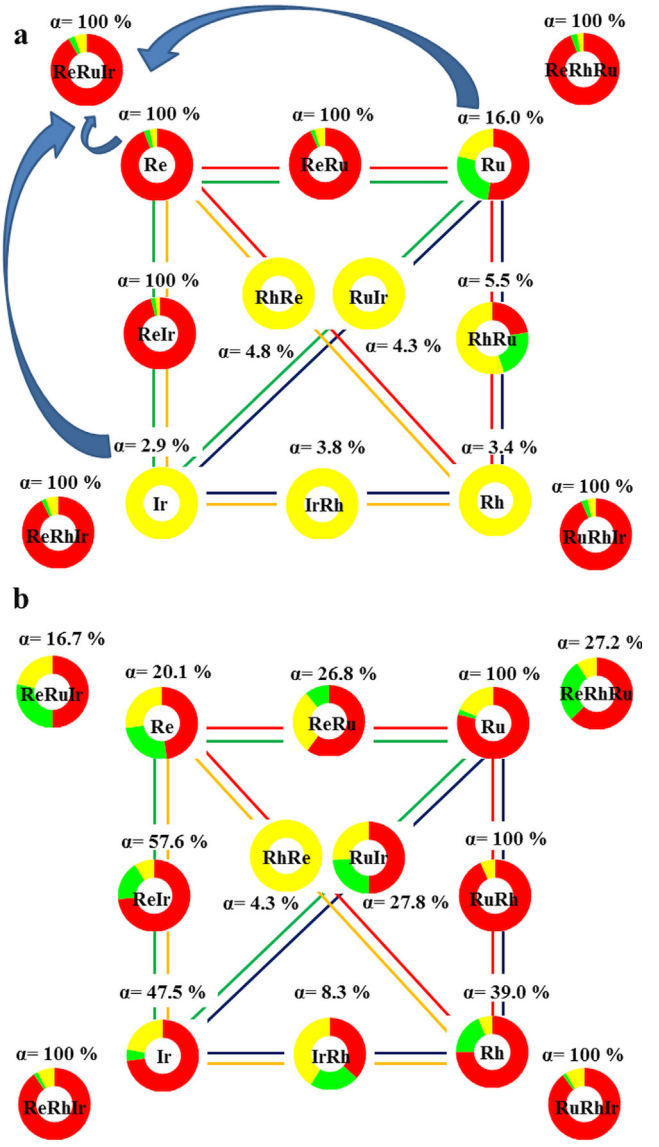

Fig. 7. A schematic illustration of the influence of metallic interactions on the conversion and selectivity of glycerol acetalization (Tables 3 and 4) for –SiO_2 (a) and—Mo (b) supported catalysts. Selectivity were indicated as follows: DDM (red)—2,2-dimethyl-1,3-dioxolane-4-methanol (solketal); DDL (green)—2,2-dimethyl-1,3-dioxane-5-ol; OPE (yellow)—3-(2-oxidanylpropan-2-yloxy)propane-1,2-diol, α—system conversion degree. The arrows in upper left side (a) indicated the preparation scheme for an example of a single three component material only. (For interpretation of the references to color in the text, the reader is referred to the web version of this article.)

vacancy of the d-bands, as this occupancy determines the adsorption strength of reactants and intermediates [37]. In particular, the electronic properties that can affect catalytic activity are work function and ionization energy (Table S4, Supplementary material). The comparison of the catalytic activity of the metals investigated in this study indicates that in fact we can find a correlation between the catalytic activity of solketal formation vs. a combination of ionization energy and electronegativity. Therefore, a low ionization energy (I) value, especially the second ionization, accompanied by a low electronegativity (χ) (electron affinity) promotes the reaction. Therefore, for example Re (760; 1260 kJ/mol (I), 1.9 (χ)) is more reactive than Rh (719; 1740 kJ/mol (I), 2.28 (χ)) or Ir (880; 1600 kJ/mol (I), 2.2 (χ)), if supported on SiO_2. In this hypothesis the Mo support should itself contribute to the activity having the advantageous I and χ values: Mo (684; 1560 kJ/mol (I), 2.16 (χ));

however. In fact, for the Mo supported catalysts we observe the activity practically for all tested samples; however; the activity level is lower than for the SiO_2 supported ones. This illustrates the importance of the SiO_2 support which can provide the acidic catalyst needed in acetalization. On the other hand, even at the low surface area Mo can significantly enhance the activity of the Ir or Rh catalysts that appeared much less reactive on the SiO_2 carrier.

4. Conclusions

We assumed that the possibility to process viscous glycerol solutions was the most important precondition for the economical treatment of waste glycerol. A high catalyst reactivity accompanied by the support of its wettability and availability should be of major importance here. Therefore, we screened nano-silica-supported Re, Ru, Ir, Rh NPs as well as various combinations of the above-mentioned metals as potential catalysts for glycerol acetalization with acetone or butanone. In fact, it was discovered that, in particular, nano-SiO_2 supported Re is a highly efficient selective catalyst of glycerol acetalization to five-membered cyclic acetals. Although Re-supported on nano-SiO_2 prefers five-membered cycles, its replacement with Mo destroys this selectivity and both five- and six-membered products were observed. Under optimal conditions, the TON that was observed significantly outperformed those that have been reported in the literature for other catalytic systems. Moreover, when tested on a larger scale, the reaction of glycerol and acetone on nano-silica-supported Re NPs provided a similar high performance and selectivity.

In summary, SiO_2-supported Re NPs can form an interesting catalytic system for glycerol acetalization in viscous liquid solutions. This seems to be especially interesting for the economical processing of glycerol wastes.

Acknowledgements

The research was co-financed by the National Research and Development Center (NCBiR) under Grant ORGANOMET No: PBS2/A5/40/2014. Maciej Kapkowski appreciates the support of the Doktoris fellowships. Authors acknowledge the technical assistance of Mrs Monika Słota and Natalia Mączka.

Appendix A. Supplementary data

Supplementary data associated with this article can be found, in the online version, at http://dx.doi.org/10.1016/j.apcatb.2016.09.032.

References

[1] C.J. Li, B.M. Trost, PNAS 105 (2008) 13197–13202.
[2] M. Besson, P. Gallezot, C. Pinel, Chem. Rev. 114 (2014) 1827–1870.
[3] C.H. Zhou, H. Zhao, D.S. Tong, L.M. Wu, W.H. Yu, Cat. Rev. Sci. Eng. 55 (2013) 369–453.
[4] D.Y. He, Z.J. Li, Z.J. Li, Y.Q. Liu, D.X. Qiu, M.S. Cai, Synth. Commun. 22 (1992) 2653–2658.
[5] B. Mallesham, P. Sudarsanam, B.M. Reddy, Catal. Sci. Technol. 4 (2014) 803–813.
[6] Z.P. Han, Y. Li, Inorg. Chem. Commun. 22 (2012) 73–76.
[7] R. Rodrigues, M. Gonçalves, D. Mandelli, P.P. Pescarmona, W.A. Carvalho, Catal. Sci. Technol. 4 (2014) 2293–2301.
[8] J.C. Meslard, F. Subira, J.P. Vairon, A. Guy, R. Garreau, Bull. Soc. Chim Fr. 1 (1985) 84–89.
[9] L. Shao, Y. Du, G. Xing, W. Lv, X. Liang, C. Qi, Monatsh. Chem. 143 (2012) 1199–1203.
[10] P. Wang, A.G. Kong, W.J. Wang, H.Y. Zhu, Y.K. Shan, Catal. Lett. 135 (2010) 159–164.
[11] W. Kantlehner, H.D. Gutbrod, B. Funke, Liebigs Ann. Chem. 2 (1980) 246–252.
[12] C. Crotti, E. Farnetti, N. Guidolin, Green Chem. 12 (2010) 2225–2231.
[13] C. Fan, C. Xu, C. Liu, Z. Huang, J. Liu, Z. Ye, Heterocycles 85 (2012) 2977–2986.
[14] C. Gonzalez-Arellano, S. De, R. Luque, Catal. Sci. Technol. 4 (2014) 4242–4249.
[15] D. Ballivet-Tkatchenko, S. Chamrey, R. Keiski, R. Ligabue, L. Plasseraud, P. Richard, H. Turunen, Catal. Today 115 (2006) 80–87.
[16] A. Piasecki, J. Am. Oil Chem. Soc. 69 (7) (1992) 639–642.
[17] P. Sudarsanam, B. Mallesham, A.N. Prasad, P.S. Reddy, B.M. Reddy, Fuel Process. Technol. 106 (2013) 539–545.
[18] B. Mallesham, P. Sudarsanam, B.M. Reddy, Catal. Sci. Technol. 4 (2014) 803–813.
[19] S. Gadamsetti, N.P. Rajan, G.S. Rao, K.V.R. Chary, J. Mol. Catal. A: Chem. 410 (2015) 49–57.
[20] P. Manjunathan, S.P. Maradur, A.B. Halgeri, G.V. Shanbhag, J. Mol. Catal. A: Chem. 396 (2015) 47–54.
[21] M.J. Silva, A.A. Julio, F.C.S. Dorigetto, RSC Adv. 5 (2015) 44499–44506.
[22] M.R. Nanda, Z. Yuan, W. Qin, H.S. Ghaziaskar, M.-A. Poirier, C. Xu, Appl. Energy 123 (2014) 75–81.
[23] B. Mallesham, P. Sudarsanam, G. Raju, B.M. Reddy, Green Chem. 15 (2013) 478–489.
[24] C.X.A. da Silva, V.L.C. Gonçalves, C.J.A. Mota, Green Chem. 11 (2009) 38–41.
[25] R. Rodrigues, M. Gonçalves, D. Mandelli, P.P. Pescarmona, W.A. Carvalho, Catal. Sci. Technol. 4 (2014) 2293–2301.
[26] C.N. Fan, C.H. Xu, C.Q. Liu, Z.Y. Huang, J.Y. Liu, Z.X. Ye, Reac. Kinet Mech. Cat. 107 (2012) 189–202.
[27] N.W. Fadnavis, G.S. Reddipalli, G. Ramakrishna, M.K. Mishra, G. Sheelu, Synthesis 4 (2009) 557–560.
[28] B. Wang, Y. Shen, J. Sun, F. Xu, R. Sun, RSC Adv. 4 (2014) 18917–18923.
[29] K.S. Rao, K. El-Hami, T. Kodaki, K. Matsushige, K. Makino, J. Colloid Interface Sci. 289 (2005) 125–131.
[30] H. Okudera, A. Hozumi, Thin Solid Films 434 (2003) 62–68.
[31] K.V. Yusenko, I.V. Korolkov, S.A. Martynova, S.A. Gromilov, Z. Kristallogr. Suppl. 30 (2009) 269–275.
[32] M. Kapkowski, P. Bartczak, M. Korzec, R. Sitko, J. Szade, K. Balin, J. Lelątko, J. Polanski, J. Catal. 319 (2014) 110–118.
[33] M. Kapkowski, T. Siudyga, R. Sitko, J. Lelątko, J. Szade, K. Balin, J. Klimontko, P. Bartczak, J. Polanski, PLoS One 11 (2015) 1–15.
[34] M. Korzec, P. Bartczak, A. Niemczyk, J. Szade, M. Kapkowski, P. Zenderowska, K. Balin, J. Lelątko, J. Polanski, J. Catal. 313 (2014) 1–8.
[35] J. Shi, Chem. Rev. 113 (2013) 2139–2181.
[36] J.M. Lorenzi, S. Matera, K. Reuter, ACS Catal. 6 (2016) 5191–5197.
[37] W.D. Wei, B.C. Sweeny, J. Qiu, J.S. DuChene, Metallic nanostructures for catalytic applications, in: Yujie Xiong, Xianmao Lu (Eds.), Metallic Nanostructures: From Controlled Synthesis to Applications, Springer Inc., New York, 2015, pp. 243–271.